JOURNAL OF MATERIALS SCIENCE 24 (1989) 618–622

Anomalous magnetic features in α-Fe_2O_3-based ceramic composites containing B_2O_3 dispersoids

S. RAM, K. A. NARAYAN*
*Advanced Centre for Materials Science and *Department of Chemical Engineering, Indian Institute of Technology, Kanpur, India*

Ceramic composites based on BaO–Fe_2O_3–B_2O_3 starting compositions have been prepared by the solid-state reaction technique. Basically the samples comprise crystalline particles due to the α-Fe_2O_3 phase. It is found that an easy control of the particle size and many of the physical properties of the system is possible by modifications of the composition and the sintering. At sintering temperatures below 1200° C the material is essentially non-magnetic. However, it exhibits surprisingly large magnetization (small particle size and low coercive fields) at sintering temperatures above 1200° C. The anomaly is explained by invoking a heat-induced $Fe^{3+} \rightleftharpoons Fe^{2+}$ reduction and considering a modified distribution of the cations in the α-Fe_2O_3 precipitated particles. The results are consistent with microstructures and electron paramagnetic resonance measurements of the samples.

1. Introduction

Ceramic/glass–ceramic composites based on BaO–Fe_2O_3 binary compositions and those precipitated from a borate glass, respectively, have been studied in relation to the development of ferrite magnets [1–3]. The B_2O_3 here behaves as a dispersive medium and also as a catalyst to allow the growth of platelet-like ferrite particles. MO–Fe_2O_3 (with M = Ca, Sr, Ba) composites in molten form are also used for the smelting and refining of metals [4].

We have studied the ferrite compositions BaO–$6Fe_2O_3$ with additions of varying amounts (up to 30 mol %) of B_2O_3 by the usual ceramic method [5]. We found that the presence of B_2O_3 in amounts greater than 5 mol % favours the growth of some non-magnetic phases. The composition series $14BaO$–$56Fe_2O_3$–$30B_2O_3$ in this regard shows the X-ray diffraction lines due to a single α-Fe_2O_3 phase (known to be antiferromagnetic). Moreover, it surprisingly gives a large magnetic moment at sintering temperatures above 1200° C. The preliminary results so obtained on the latter composition are reported in this article.

2. Experimental procedure

The raw materials of $BaCO_3$, Fe_2O_3 and H_3BO_3 mixed together in stoichiometric ratio are ground into a fine powder by milling in a ball mill for 10 h using acetone. The specimens (pressed as pellets) are then sintered in air at 900 to 1500° C for several hours. Their X-ray powder diffraction patterns are recorded on a Rich and Seifert Isodebyeflex 2002 diffractometer using filtered Cr$K\alpha$ radiation. The microstructures are analysed with a Zeiss optical microscope and a Bausch and Lomb image analyser (Model 500).

The magnetization measurements are performed with a PAR vibrating-sample magnetometer (Model 150) in conjunction with a Varian V-7200 magnet. Electron paramagnetic resonance (EPR) spectra are measured on a Varian Associates spectrophotometer (Model V-4502-12) in the X-band frequency region.

3. Results and discussion

3.1. Microstructures and X-ray diffraction analysis

The composition series represented by $14BaO$–$(86-x)Fe_2O_3$–xB_2O_3 exhibits crystalline phases due to (i) barium-ferrites, (ii) $BaFe_2O_4$, and (iii) Fe_2O_3 when the samples are sintered between 900 and 1500° C. The reaction appears very sensitive to the B_2O_3 content. It favours the growth of the α-Fe_2O_3 phase for $x > 5$ (and barium ferrites for $x < 5$). The α-Fe_2O_3 particles so produced are thermally stable. They do not convert into γ-Fe_2O_3 (a magnetic phase) or react with $BaFe_2O_4$ to give rise to any other magnetic phase, even if the reaction is continued for several days.

The yield of α-Fe_2O_3 in the reaction increases with increasing amount of B_2O_3. The specimens (Fig. 1) of the composition containing 30 mol % B_2O_3 as a consequence reveal the diffraction lines characteristic of only the α-Fe_2O_3 phase for any of the heat treatments (Table I). The peak intensities, bandwidths and d values of the lines vary considerably, however, possibly due to variations in particle size (cf. Table II below) and morphology. This is consistent with the microstructures of the samples shown in Figs 2 and 3.

The particle size in general ranges from a few tenths of a nanometre to ~ 10 nm. Because of the severe overlap of the Bragg diffraction lines it is not possible to carry out a size distribution analysis [6]. Therefore, we have evaluated the mean diameters of the platelet-like particles following the Langford analysis [7]. Some ten diffraction lines in the range $30° \leqslant 2\theta \leqslant 150°$ have been fitted to Voigt functions from which the integral width (β) is estimated. The corresponding

0022–2461/89 $03.00 + .12

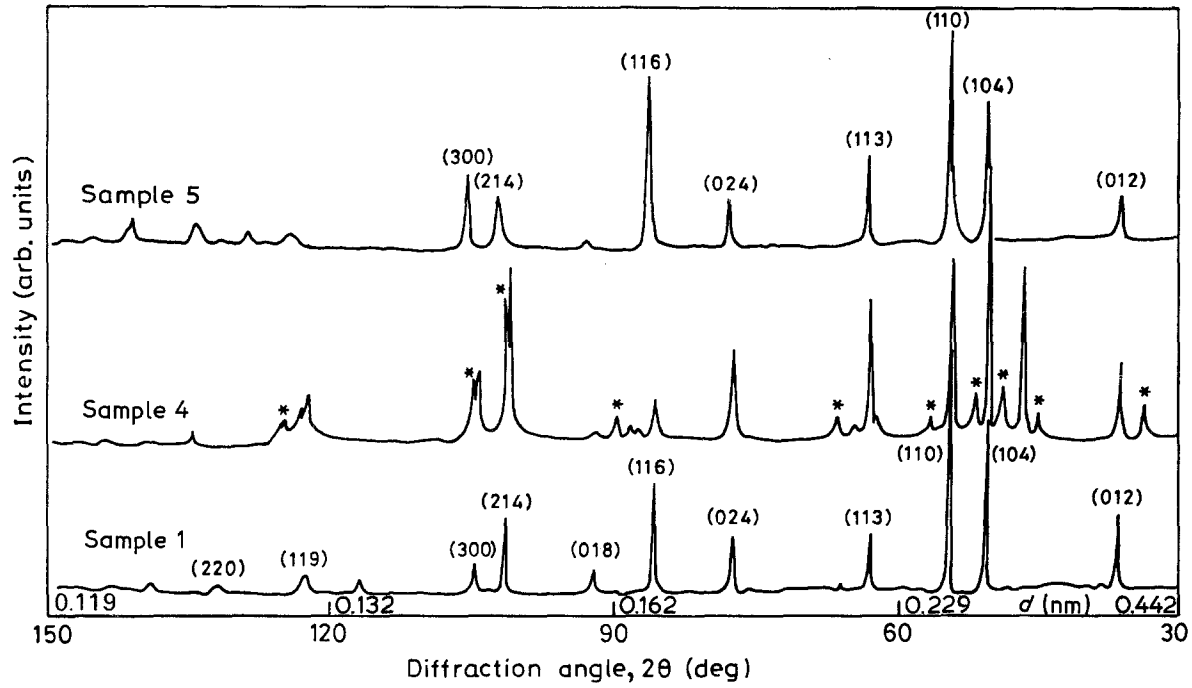

Figure 1 X-ray powder diffraction patterns of Samples 1, 4 and 5. The peaks marked by the $(h\,k\,l)$ values refer to α-$Fe^{3+}_{2-x}Fe^{2+}_{x}O_{3-(x/2)}$ crystallites. *Traces of $BaFeO_{3-x}$ phase.

TABLE I Magnetic characteristics and postulated compositions for $Fe^{3+}\uparrow(Fe^{3+}_{1-x}Fe^{2+}_{x})\downarrow O_{3-(x/2)}$ crystallites precipitated in the various ceramic composites

Sample No.	Heat treatment	Magnetization results			Composition and magnetic distribution (postulated)*		
		ϱ_s (e.m.u. g^{-1})	ϱ_r/ϱ_s	H_c (O_e)	x	n_B	θ_c
1	1000° C, 20 h	0.35	0.51	510	0	0.024	179.715
2	1100° C, 20 h	0.30	0.50	530	0	0.021	179.715
3	1200° C, 20 h	0.25	0.56	560	0	0.017	179.716
4	1300° C, 35 h	6.80	0.05	47	0.5	0.47	179.95
5	1400° C, 10 h	23.0	0.22	213	0.8	1.57	161.2
6	1465° C, 10 h	25.0	0.22	260	0.8	1.71	158.9
7	1500° C, 10 h	24.5	0.24	275	0.8	1.68	159.4

*x is determined by chemical analysis. θ_c is the canting angle calculated by using the observed ϱ_s (in Bohr magneton number n_B) per formula unit and composition of $Fe^{3+}_{2-x}Fe^{2+}_{x}O_{3-(x/2)}$ crystallites.

mean diameter D is calculated from $D = \lambda/\beta \cos\theta$ [7]. The results are reported in Table II. We find that the particle sizes deduced from X-ray analysis fit very well with those observed in micrographs. These results and the data in Tables I and II clearly demonstrate that the particle size and the hence intrinsic properties of the systems can be significantly modified by thermal treatment.

The platelet-like morphology of the particles is confirmed by the X-ray diffraction patterns of powder and bulk samples. A diffraction line (2 2 0) that appears weakly in the powder samples exhibits a prominent intensity in the bulk. Moreover, the (1 1 0) or/and (1 0 4) lines usually show the strongest intensity in the powder. This implies that the c axis in the individual particles (the crystal structure is essentially rhombohedral with space group $D^6_{3d}R_{\bar{3}c}$ and lattice parameters $a = 0.503$ nm, $c = 1.375$ nm and $Z = 6$ [8]) is grown parallel to the bulk surface.

In optical micrographs, the crystallite particles (white) in the different samples exhibit almost similar patterns. They must therefore belong to the same crystalline phase, as is also evident from X-ray diffraction. The individual particles in a sample, however, differ in colour and intensity as measured with a polarizer using reflected light. The micrograph so recorded for Sample 5 is shown in Fig. 3b. The structure looks completely different from that recorded (Fig. 3a) without a polarizer. The features also vary with the orientation of the polarizer. This is likely if

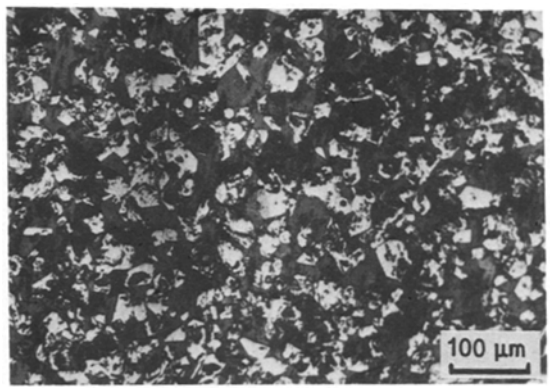

Figure 2 Microstructures showing the precipitation of platelet-like α-Fe_2O_3 particles (white) in Sample 1.

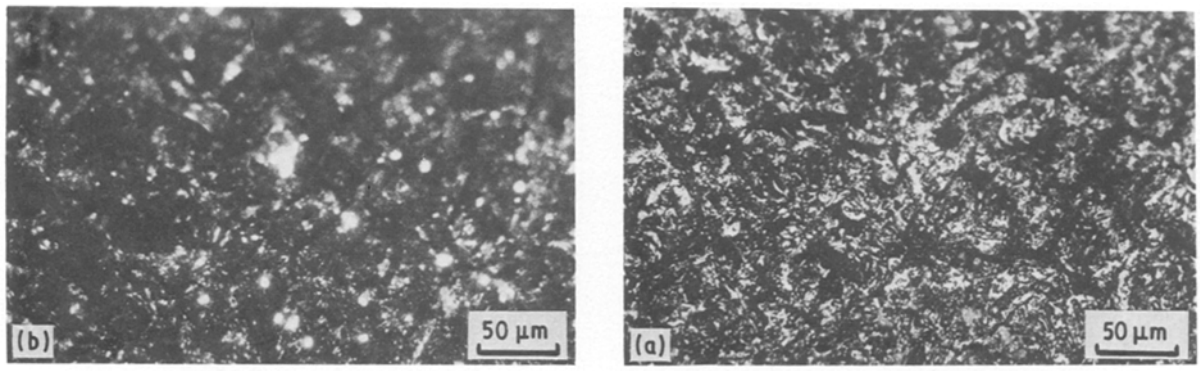

Figure 3 Optical micrographs of Sample 5 recorded (a) without and (b) with a polarizer.

the crystalline particles (of a rhombohedral crystal lattice) are grown with no specific orientations for the *a* and *b* axes (though the *c* axis grows lying parallel to the bulk surface) in the particle.

3.2. Magnetic properties

The saturation magnetization ϱ_s and coercive field H_c obtained as a function of the sintering temperature are shown in Fig. 4. ϱ_s shows little temperature dependence below 1200° C and gives a maximum of $\varrho_s \sim 0.35$ e.m.u. g^{-1} (very close to ~ 0.4 e.m.u. g^{-1} reported for α-Fe_2O_3 crystals [9]). After that the magnetization sharply rises with increasing temperature. It attains an almost fixed value of ~ 25 e.m.u. g^{-1} for sintering around 1400° C.

The anomalously large ϱ_s precipitated in Samples 5 to 7 can be accounted for by invoking a heat-induced reduction reaction of ferric ions, i.e.

$$Fe^{3+} + Q \rightleftharpoons Fe^{2+} - e^- \qquad (1)$$

in the α-Fe_2O_3 particles during sintering at relatively high temperatures. Haberey [3] has also reported Fe^{3+} reduction in BaO–Fe_2O_3–B_2O_3 glass systems when melting at around 1350° C. The actual composition in the particles therefore appears due to the α-$Fe^{3+}_{2-x}Fe^{2+}_x O_{3-(x/2)}$ phase. In α-Fe_2O_3 (antiferromagnetic) the magnetic spins of the two Fe^{3+} ions are coupled in an antiparallel scheme

$$(Fe^{3+})^A \uparrow (Fe^{3+})^B \downarrow O_3 \qquad (2)$$

and the effective ϱ_s is zero [8]. If we consider a similar magnetic distribution also for the α-$Fe^{3+}_{2-x}Fe^{2+}_x O_{3-(x/2)}$ particles and assume that the $Fe^{3+} \rightleftharpoons Fe^{2+}$ reduction occurs only in one type (A or B) of the two lattice sites, we would have an effective magnetization given by

$$\begin{aligned} \varrho_s &= \varrho_a(Fe^{3+})^A - \varrho_b(Fe^{3+}_{1-x}Fe^{2+})^B \\ &= x\mu_B \end{aligned} \qquad (3)$$

Here the moments of Fe^{3+} and Fe^{2+} are taken to be $5\mu_B$ and $4\mu_B$, respectively (where μ_B is the magnetic moment).

In the above scheme x could take a value up to unity and that would give a maximum ϱ_s of $1\mu_B$. It is much smaller than the observed values at 295 K (cf. the data in Table I). The discrepancy ensures that a magnetic spin canting is expected between the sublattice magnetizations ϱ_a and ϱ_b. Also the α-Fe_2O_3 crystals show a residual magnetization due to this effect, operative above the so-called magnetic transition temperature $T_m \sim 260$ K [8–10]. We have estimated the canting angle θ_c to be 179° (at ~ 295 K) for the α-Fe_2O_3 particles and a variation in the narrow range of 159 to 161° for the Fe^{2+}-substituted α-Fe_2O_3 particle systems (cf. Table I). This is done simply by using the observed ϱ_s in the equation

$$\begin{aligned} (\varrho_s)_{obs.} &= [\varrho(Fe^{3+})^A] \cdot [\varrho(Fe^{3+}_{1-x}Fe^{2+}_x)^B] \\ &= \varrho_a^2 + \varrho_b^2 + 2\varrho_a\varrho_b \cos\theta_c \end{aligned} \qquad (4)$$

Another striking feature of the results is the variation of H_c (Fig. 4) with sintering temperature and its sudden fall in a particular sample (No. 4) sintered at 1300° C. It may be accounted for by a shape anisotropy H_b in the platelet-like precipitated particles, i.e.

$$H_c = H_a - (N_c - N_a)\varrho_s \qquad (5)$$

where $H_a = 2K_1/\varrho_s$ is the magnetocrystalline anisotropy field, k_1 is a constant and N_c and N_a are the demagnetization factors parallel and perpendicular to

TABLE II Summary of microstructural and EPR results

Sample No.	Particle size (μm)*		*g* value	Linewidth ΔH (O_e)	*I* (arb. units)
	MS	XD			
1	20	21	4.47	125	0.4×10^{-5}
3	25	27	4.45	100	0.9×10^{-5}
4	17	13	1.92	1200	17×10^{-5}
5	5	5	3.84, 1.60	2800, 750	1, 0.04
6/7	3	4	3.84, 1.60	2800, 850	0.95, 0.08

*Sizes measured by microstructure (MS) and calculated from X-ray diffraction results (XD). They correspond to the mean diameter of platelet-like particles.

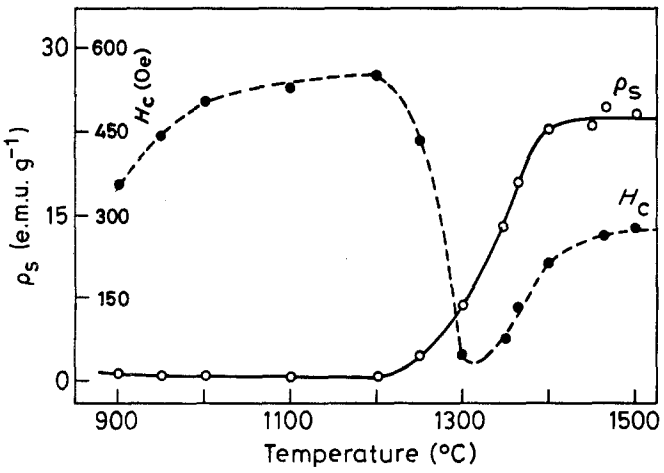

Figure 4 (○) Maximum saturation magnetization ϱ_s and (●) coercivity H_c obtained for the various samples as a function of sintering temperature.

the c axis, respectively. The factors N_c and N_a would remain practically unchanged for a system of sufficiently flat particles, as precipitated in Samples 1 to 4 (particle size $\sim 20\,\mu$m). The discontinuity (small H_c value) in the H_c plot could arise therefore due to an enhanced ϱ_s precipitation (small H_a and large H_b values) for sintering at around 1300° C. For sintering at higher temperatures the values of ϱ_s (~ 25 e.m.u. g^{-1}) and also H_a become almost fixed, and H_c is solely governed by the demagnetization factors. Particles of much reduced size (to $\sim 4\,\mu$m average value) are observed in these samples. A marginal variation of their H_c values may therefore be interpreted within the scope of the superparamagnetic theory of uniaxial fine particles [11].

3.3. EPR results

In order to be able to comment on the growth of highly magnetic centres (Fe^{3+}/Fe^{2+}) in the particles precipitated as a function of the sintering temperature we carried out EPR measurements on these samples. Typical spectra are shown in Fig. 5. The corresponding data for g value, linewidth ΔH and integrated intensity I estimated for unit mass of the sample are given in Table II.

The results successfully account for the precipitation of large magnetic moments that are reflected in the modified resonance intensities in the later samples (Nos 5 to 7). Sample 1, which comprises particles due to a weakly ferromagnetic α-Fe_2O_3 phase, shows a very weak moment ($I = 0.4 \times 10^{-5}$ units) and sharp resonance at $g = 4.47$. This is characteristic of Fe^{3+} species forming paramagnetic centres [2]. Also a peak of $g \sim 2$ appears in Samples 5 to 7 containing α-$Fe^{3+}_{2-x}Fe^{2+}_x O_{3-(x/2)}$ precipitated particles. This exhibits a characteristically large ΔH (~ 1200 Oe) and much enhanced intensities (I). The features could be ascribed to ferrimagnetic resonance exhibited by Fe^{3+}/Fe^{2+} ions in different interstitial sites [12].

The spectrum in Sample 5 (also Samples 6 and 7) in fact comprises several overlapping resonances in the region from $g \sim 10$ to 0.5. This is indicative of various magnetic centres (Fe^{3+}/Fe^{2+}) being present in both octa- and tetrahedral coordination sites [13]. These sites are essentially distorted and as a matter of fact impart (i) a large asymmetry to the resonance band profile, and (ii) a drastically modified (by a factor $\sim 10^5$) resonance intensity. The relatively fine particles ($\sim 4\,\mu$m size) found in these samples could also have an input to the line-broadening and band shape asymmetry of the resonance.

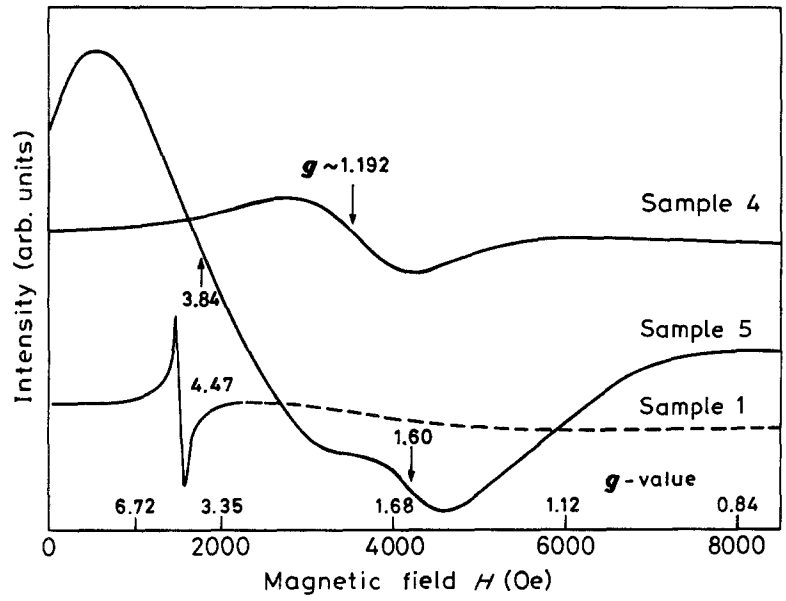

Figure 5 EPR spectra of the various samples.

References

1. A. COLLOMB, P. WOLFERS and X. OBRADORS, *J. Magn. Magn. Mater.* **62** (1986) 57.
2. S. RAM, D. CHAKRAVORTY and D. BAHADUR, *ibid.* **62** (1986) 221.
3. F. HABEREY, *IEEE Trans. Magn.* **MAG 23** (1987) 29.
4. S. SUMITA, K. MORINAGA and T. YANAGASE, *Trans. Jpn Inst. Metals* **24** (1983) 35.
5. S. RAM, D. BAHADUR and D. CHAKRAVORTY, *J. Magn. Magn. Mater.* **71** (1988) 359.
6. B. E. BARREN and B. L. AVERBACH, *J. Appl. Phys.* **21** (1950) 595.
7. J. I. LANGFORD, *J. Appl. Crystallogr.* **11** (1978) 10.
8. N. YAMAMOTO, *J. Phys. Soc. Jpn* **24** (1968) 25.
9. G. SHIRANE, S. J. PICKART, R. NATHANS and Y. ISHIKAWA, *J. Phys. Chem. Solids* **10** (1959) 37.
10. Q. A. PANKHURST, C. E. JOHNSO and M. F. THOMAS, *J. Phys. C* **19** (1986) 7081.
11. A. HERPIN, "Theorie due Magnetisme" (Presses Universitaires de France, 1968) p. 105.
12. S. SMIT and H. P. J. WIJN, "Ferrites" (Wiley, New York, 1959) p. 87.
13. D. LOVERIDGE and S. PARKE, *Phys. Chem. Glasses* **12** (1971) 19.

Received 10 December 1987
and accepted 6 May 1988